Turkish Journal of Earth Sciences

http://journals.tubitak.gov.tr/earth/

Research Article

Turkish J Earth Sci
(2023) 32: 975-988
© TÜBİTAK
doi:10.55730/1300-0985.1887

The geo/thermochronology of Dismal Island (Marguerite Bay, Antarctic Peninsula)

Fatih KARAOĞLAN[1,2,*], Burcu KARATAŞ[1], Yavuz ÖZDEMİR[3], Erhan GÜLYÜZ[3,4], Oleg VASSILEV[5], Mahmut Oğuz SELBESOĞLU[6], Semih GİLDİR[1]

[1]Geological Engineering Department, Engineering Faculty, Çukurova University, Adana, Turkiye
[2]Department of Geological Processes, Institute of Geology, Czech Academy of Sciences, Praha, Lysolaje, Czech Republic
[3]Geological Engineering Department, Engineering Faculty, Van Yüzüncüyıl University, Van, Turkiye
[4]Department of Neotectonics and Thermochronology Institute of Rock Structure and Mechanics of the Czech Academy of Science, Prague 8 Czech Republic
[5]Bulgarian Antarctic Institute, Sofia, Bulgaria
[6]Department of Geomatics Engineering, Engineering Faculty, İstanbul Technical University, İstanbul, Turkiye

Received: 11.05.2023 • **Accepted/Published Online:** 16.11.2023 • **Final Version:** 28.11.2023

Abstract: Dismal Island is located at the entrance of Marguerite Bay between Adelaide Island to the northeast and Alexander Island to the southwest within the Antarctic Peninsula (AP). Its unique position between Alexander and Adelaide islands provides the opportunity to perform testing and link these regions through Cenozoic magmatism and tectonics due to the subduction of the Pacific plate beneath the AP along the northern margin.

Dismal Island was visited in February 2021 within the framework of the sixth Turkish Antarctic Expedition (TAE-VI). Thirteen samples were collected for petrography, geochronology, and low-temperature thermochronology (LTT). Of the samples, 3 were dated using laser ablation-inductively coupled plasma-mass spectrometer zircon U-Pb geochronology, 2 were dated using apatite fission-track (AFT) analysis, and 1 was dated using apatite uranium-thorium-helium (U-Th/He) (AHe) thermochronology.

The island comprises massif quartz-diorite, tonalite, mafic, and felsic dikes, indicating a hybrid magma source. The 3 zircon U-Pb ages yielded a crystallization age of 47–48 for the magmatic body. The AFT ages yielded a cooling age of 41 Ma, suggesting either a shallow emplacement at a depth of ~4 km or an uplift/exhumation during middle-late Eocene boundary. In contrast, the AHe age of 1 sample was 20.1 ± 1.1 Ma, together with a fast-cooling profile during the same period, which indicated an early Miocene uplift in the region.

Similar early-middle Eocene crystallization ages within similar rock outcrops were determined on Adelaide and Alexander islands, Adelaide Island Intrusive Suite. The AFT ages obtained in this study (~41 Ma), close to formation age, were also found on Adelaide and Alexander islands. The (LTT) literature of the region shows that the LTT ages get younger to the north along the AP, reflecting the northward migration of the ridge-trench collision and opening of the slab window along the western coast of the AP. The AHe age and the fast-cooling profile suggested that the ridge-subduction between the Tula and Adelaide fracture zones to the north of Dismal Island reached the region during Aquitanian-Burdigalian.

Key words: Antarctic Peninsula, Dismal Island, zircon U-Pb, apatite fission-track, apatite U-Th/He, ridge-trench collision

1. Introduction

The Antarctic Peninsula (AP), extending over 1500 km from Antarctica toward South America, between the southeast Pacific Ocean and the Weddell Sea, forming the northernmost portion of the Antarctica continent, was located along the continental margin of Gondwana until the early Mesozoic before its breakup (Dalziel, 1982; Lawver et al., 1992; Storey and Granot, 2021). Moreover, the AP has witnessed continuous subduction, accretion, and collision events since the Paleozoic (Vaughan and Storey, 2000; Burton Johnson and Riley, 2015; Bastias et al., 2020; Jordan et al., 2020; Storey and Granot, 2021).

The AP can be divided into 3 major tectonic units, including 7 terrains (Vaughan and Storey, 2000) (Figure 1). The Western Domain comprises the LeMay Group, Scotia Metamorphic Complex, and Fossil Bluff Group. The Central Domain, separated from the Western Domain by the George VI Sound, consists of products of the magmatic arc units formed between the Silurian and Cretaceous. The Eastern Domain, separated from the Central Domain by the Eastern Palmer Land Shear Zone (EPLSZ), represents the late Paleozoic margin of Gondwana and consists of the Latady Group and Larsen Group (Macdonald et al., 1999; Vaughan and Storey, 2000; Millar et al., 2002; Willan, 2003;

* Correspondence:fkaraoglan@cu.edu.tr

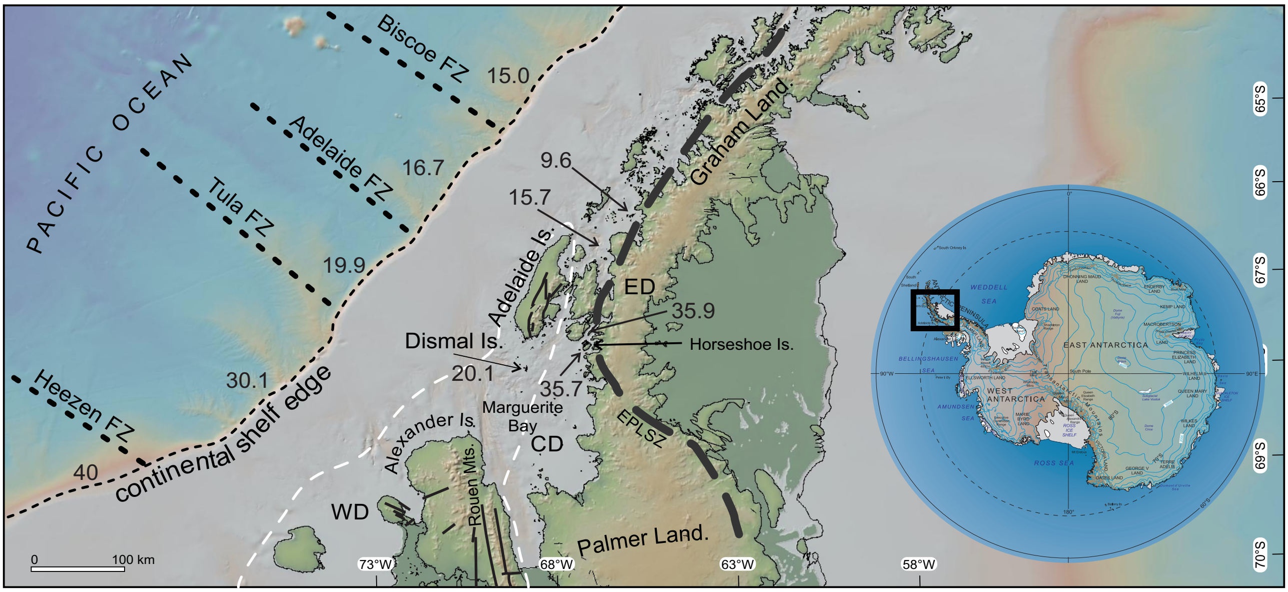

Figure 1. Location of Dismal Island within the AP showing the timing of the ridge-trench collision along the Antarctic continental shelf edge (numbers on the dashed line indicate the timing of the ridge-trench collision, numbers on the AP show the AHe ages in Ma); EPLSZ: Eastern Palmer Land Shear Zone, ED: Eastern Domain, CD: Central Domain, WD: Western Domain; white dashed line shows the margins of the Western Domain; EPLSZ separates the CD from the ED (base map: GMRT v4.11; inside map: location map showing the context of the study area within Antarctica, map from LIMA: http://lima.usgs.gov)

Vaughan et al., 2012; Bastias et al., 2020). The Paleozoic-Cenozoic arc system, which covered the entire AP, was developed above an eastward-dipping Paleo-Pacific subduction zone (Burton Johnson and Riley, 2015; Storey and Granot, 2021). Extensive crustal growth in the region was initially supported by the Gondwana break-up, which is marked by early-middle Jurassic magmatism and was enhanced by the continued/renewed subduction system(s) with arc, forearc, and backarc sequences deposited mostly during the early-late Cretaceous in an extensional setting (Leat et al., 1995; Riley and Leat, 2021).

The Cenozoic events in the AP are summarized by a progressive transition from an active to an inactive subduction zone along its western margin. The transition and the subduction termination are associated with the gradual subduction of the Antarctic-Phoenix spreading center during the Cenozoic. The segmented structure of the spreading center and its oblique position with respect to the subduction axis are the reasons behind its gradual subduction pattern (Hole and Larter, 1993; Larter et al., 1997; Eagles, 2004; Breitsprecher and Thorkelson, 2009) (Figure 1).

Marguerite Bay is located in the southern part of the Central Domain to the north of Palmer Land, hosting many archipelagos, islets, and islands (Figure 1). Dismal Island was visited as part of the sixth Turkish Antarctic Expedition (TAE-VI) during January–March 2022 (Figure 2). The target destination of the TAE-6 was Horseshoe Island, where the temporary Turkish Base (and potential future permanent Turkish Base) was established (Figure 1).

Dismal Island is the biggest island, measuring ~7 km^2 within an archipelago formed by 21 islets and islands located at the entrance of Marguerite Bay, closer to Adelaide Island (Figures 1 and 2). Marguerite Bay is a major embayment on the Pacific coast of the AP, between Adelaide Island to the north and Alexander Island to the south, with dimensions of approximately 175 km N–S and 150 km E–W, located in between Graham Land to the north and Palmer Land to the south of the AP (Wyeth, 1977) (Figure 1). Adelaide and Alexander islands form the major components of the Western Domain in the region (Figure 1).

Adelaide Island comprises late Mesozoic-Cenozoic sedimentary, volcanoclastic, and volcanic rocks formed in the forearc to intraarc setting included in the Western Domain (Riley et al., 2012). The oldest unit of this arc setting, the Buchia Buttress Formation, includes volcanic breccias, tuffs, and volcaniclastic rocks alternated with coarse-grained sandstone and conglomerates. This unit is overlain by Aptian–Albian-aged sedimentary rocks, volcanoclastic, and volcanic rocks (Milestone Bluff Formation). There are 3 formations, the Reptile Ridge, Bond Nunatak, and Mount Liotard, which are Maastrichtian in age, that unconformably overlie the Milestone Bluff Formation. The Reptile Ridge Formation

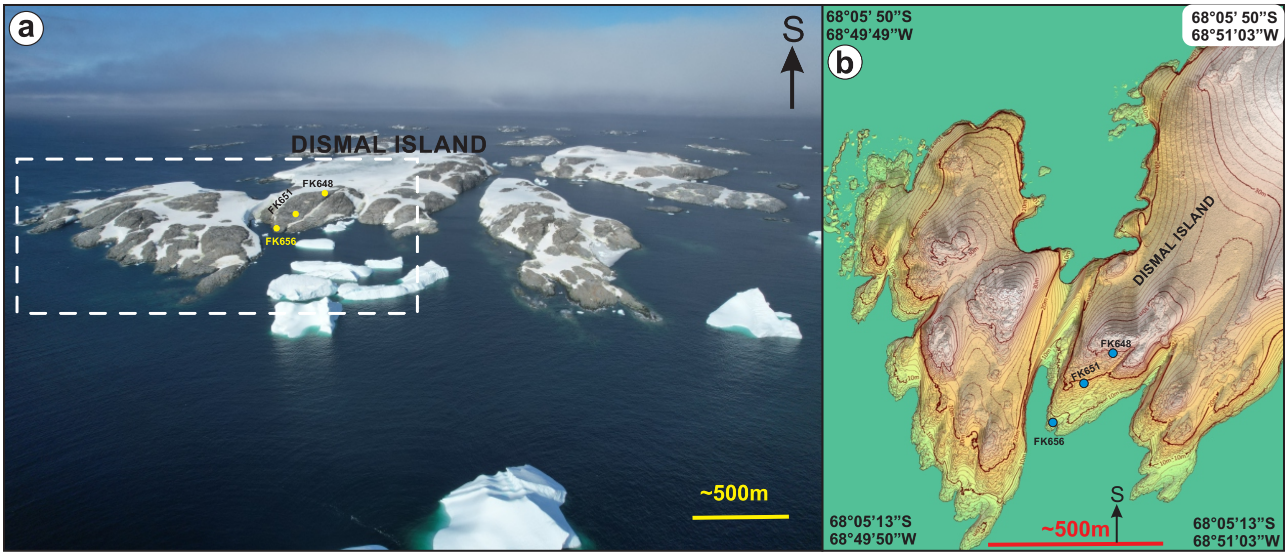

Figure 2. (a) Aerial view of Dismal Island, (b) digital elevation model obtained from a unmanned aerial vehicle photogrammetry survey in postprocessing kinematic mode. The model was based on 2765 images, each at 20 Mp, producing a ground sampling distance of 2 cm/pixel.

comprises rhyolitic ignimbrites and lithic tuffs. The Bond Nunatak Formation comprises basaltic volcanic rocks interbedded with coarse-grained sandstones and conglomerates. The Mount Liotard Formation comprises basaltic andesite interbedded with sedimentary rocks. The youngest magmatic unit on the island is Adelaide Island Intrusive Suite, which comprises granodiorite, tonalite, diorite, gabbro, and quartz monzonite associated with felsic and dolerite dikes. Leucocratic granodiorite and hybrid gabbro/granodiorite plutons are the most abundant on Adelaide Island, which are dated to 52–45 Ma (Riley et al., 2012).

Alexander Island is tectonically situated in a forearc setting within the Western Domain of the AP, located at the southern part of Marguerite Bay. It hosts the LeMay Group and the mid-Jurassic to mid-Cretaceous Fossil Bluff Group. These groups are separated by a dextral strike-slip fault associated with the oblique subduction of the Phoenix Plate (Butterworth et al., 1988; Storey and Nell, 1988; Doubleday et al., 1993; Larter et al., 1997; Twinn et al., 2022). Adelaide Island, which sits on the overriding plate of a convergence system, represents the Mesozoic-Cenozoic volcanic arc system and accretionary prism products of the AP, including sedimentary and volcanic succession intruded by plutons (Griffiths and Oglethorpe, 1998; Riley et al., 2012).

To the south of the study area, the ridge-trench collision between the Antarctic–Phoenix ridge segments and the former trench along the AP margin above Alexander Island occurred c. 44–30 Ma (Hole and Larter, 1993; Twinn et al., 2022). The thermochronology data shows an accelerated cooling on Alexander Island between 40 and 35 Ma (Storey et al., 1996; Twinn et al., 2022). The ridge subduction moved toward the north and reached between the Heezen and Tula fracture zones between 40 and 30 Ma and continued to the Tula and Adelaide fracture zones between 30 and 20 Ma (Hole and Larter, 1993; Hole et al., 1994; Johnson, 1997; Larter et al., 1997; Guenthner et al., 2010; Twinn et al., 2022). The ongoing subduction reached north of Dismal Island between the Tula and Adelaide fracture zones at ~20 Ma (Hole and Larter, 1993; Larter et al., 1997; Breitsprecher and Thorkelson, 2009) (Figure 1). The ridge-trench collision and the slab-window migrated toward the northeast along the trench and reached the South Shetland Islands during the late Miocene (Larter et al., 1997; Breitsprecher and Thorkelson, 2009; Guenthner et al., 2010; Clinger et al., 2020). The available thermochronology data shows that the ages get older away from the continental shelf margin and become unrelated to the latest ridge-trench collision (Guenthner et al., 2010; Clinger et al., 2020; Twinn et al., 2022) (Figure 1).

This study aimed to enlighten the time-progressive evolution of Dismal Island within Graham Land on the AP, located in the Western Domain. The results link subduction processes along the western margin of the AP to the Cenozoic geodynamic evolution of the southern part of the AP. This study presents the first laser ablation-inductively coupled plasma-mass spectrometer (LA-ICP-MS) zircon U-Pb, apatite fission-track (AFT), and apatite uranium-thorium-helium (U-Th/He) (AHe) ages from Dismal Island. The data obtained herein showed Eocene magmatism emplaced in an Upper Cretaceous lower crust and uplifted in a ridge-trench collision setting closely related to the subduction processes along the western margin of the AP, which has continued since the Paleozoic.

2. Materials and methods

2.1. Sampling

The TAE-VI team embarked on the island's northern edges, and a small portion of the island was accessible for field observation (Figure 2). A massive magmatic body cut by felsic and mafic dikes is the only outcrop on the island (Figures 3a–3e). Thirteen samples were collected from the fresh outcrops of the intrusive rocks and dikes (Table 1).

The major component of the island is formed by tonalite, q-diorite, and gabbro, whereas both felsic and mafic dikes were mechanically altered and observed as boulders in all of the outcrops (Table 1, Figure 3).

2.2. Petrography

Thin sections were prepared before petrographic investigations at the Thin Section Laboratory of the Geological Engineering Department of Çukurova University. The petrographic investigations were performed using a Leica polarized microscope (Leica Microsystems, Wetzlar, Germany) at the Petrography Laboratory of the Geological Engineering Department of Van Yüzüncü Yıl University.

2.3. Zircon U-Pb analyses

The mineral separation, including crushing, sieving, magnetic, and heavy liquid separation, was performed at the Geological Engineering Department of Çukurova University, Adana Türkiye. The LA-ICP-MS zircon U-Pb analyses were done at the Geological Processes Department of the Geology Institute of the Czech Academy of Sciences, Prague (Czech Republic) using an Element 2 high-resolution sector field MS (Thermo Fisher Scientific Inc., Waltham, MA, USA) coupled with a 193-nm ArF Analyte Excite excimer LA system (Teledyne/Cetac) equipped with a HelEx II active 2-volume ablation cell. The data acquisition included a 20-s background measurement followed by 40-s sample ablation. The laser was used in single-spot mode with a spot size of 25–40 μm with 3–4 J/cm^2 of energy at a repetition rate of 4 Hz. He and N_2 gases were used to carry the ablated material to the ICP-MS. The ICP-MS was used in time-resolved mode and was calibrated using the standard glass National Institute of Standards and Technology (NIST) 612 to obtain the maximum U^+ signals with a ThO/Th ratio <0.5%. Ar gas was used for the plasma gas, and during the analyses, ^{204}Pb, ^{206}Pb, ^{207}Pb, ^{208}Pb, ^{232}Th, ^{235}U, and ^{238}U isotopes were measured at 10, 15, 30, 10, 10, 20, and 10 ms, respectively. Zircon 91500 was used as the primary reference material, and the Plesovice and GJ-1 reference zircons were used as secondary reference materials within the sample batch to test the accuracy and external reproducibility (Wiedenbeck et al., 2004; Slama et al., 2008). Iolite v 4.0 data processing software was used for data reduction and processing (Paton et al., 2011).

2.4. Apatite (U-Th)/He analyses

AHe analyses were performed at the Institute of Rock Structure and Mechanics of the Czech Academy of Sciences, Prague (Czech Republic). At least 3 inclusion and crack-free euhedral crystals were analyzed for each sample. The crystal images were taken at 2 different orientations to measure the dimensionsof each grain to calculate the α-ejection corrections factors (Farley et al., 1996; Farley, 2002) for the age calculations. A fully

Table 1. Locations of the collected samples.

Sample	Location	Latitude	Longitude	Altitude (m)	Rock unit
FK648	Dismal Island	S68° 5′ 30.473″	W68° 50′ 46.082″	24	q-diorite
FK649a	Dismal Island	S68° 5′ 29.32″	W68° 50′ 45.51″	24	q-diorite
FK649b	Dismal Island	S68° 5′ 29.321″	W68° 50′ 45.51″	24	tonalite
FK650a	Dismal Island	S68° 5′ 28.414″	W68° 50′ 43.818″	21	q-diorite
FK650b	Dismal Island	S68° 5′ 28.414″	W68° 50′ 43.818″	21	dike – micro gabbro
FK651	Dismal Island	S68° 5″ 28.072″	W68° 50′ 43.022″	24	dike – micro gabbro
FK652	Dismal Island	S68° 5′ 27.92″	W68° 50′ 42.796″	25	dike – aplite
FK653a	Dismal Island	S68° 5′ 26.768″	W68° 50′ 43.634″	18	tonalite
FK653b	Dismal Island	S68° 5′ 26.768″	W68° 50′ 43.634″	18	q-diorite
FK653c	Dismal Island	S68° 5′ 26.768″	W68° 50′ 43.634″	18	q-diorite
FK654	Dismal Island	S68° 5′ 31.891″	W68° 50′ 37.763″	17	q-diorite
FK655	Dismal Island	S68° 5′ 25.901″	W68° 50′ 39.934″	11	q-diorite
FK656	Dismal Island	S68° 5′ 23.125″	W68° 50′ 40.7″	0	q-diorite

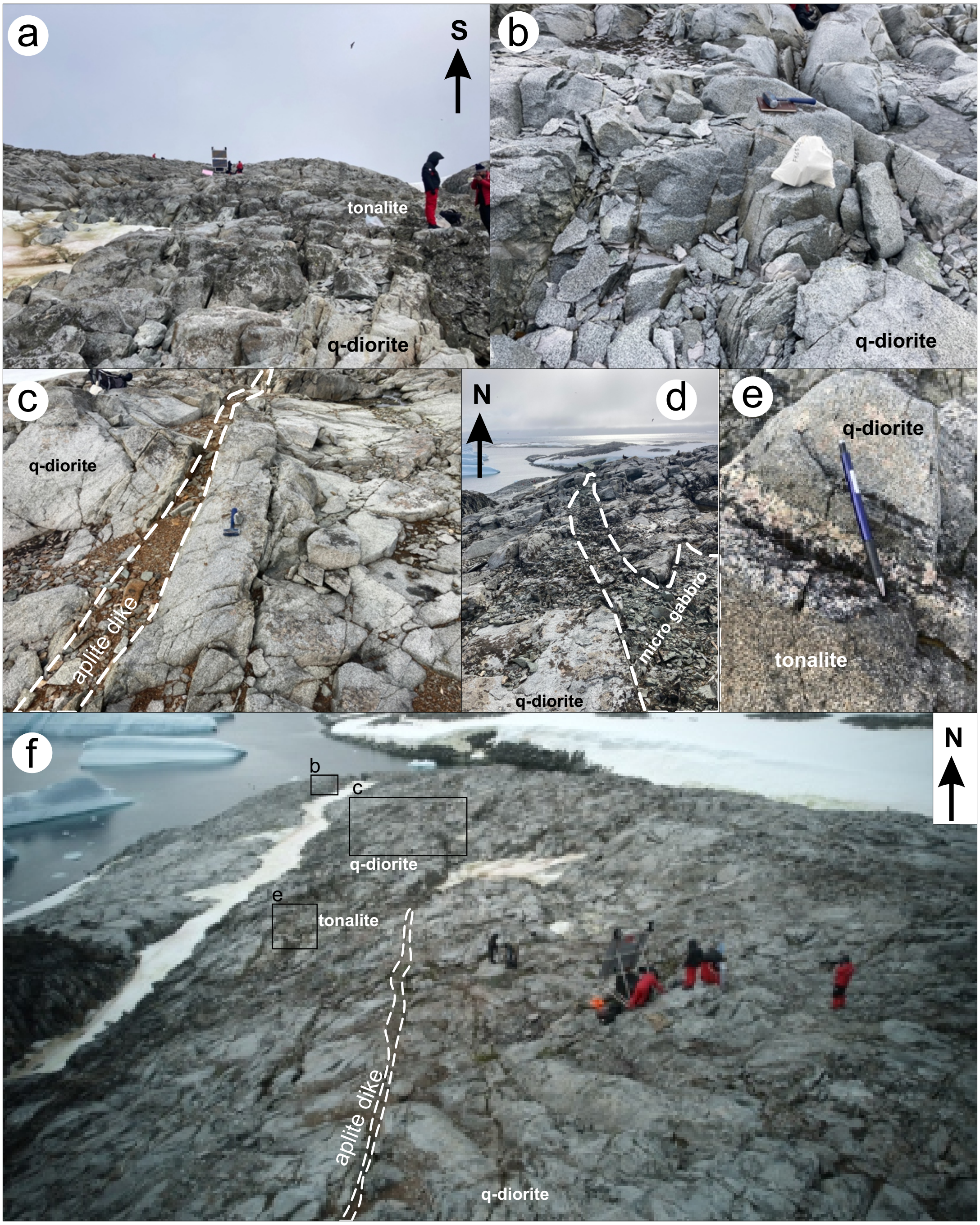

Figure 3. Field views from Dismal Island. (a,b,e) General outcrop of the major unit (Q-diorite); (c) felsic dike (aplite); (d) mafic dike (micro gabbro); (f) general view of the northern face of Dismal Island. The rocks of the dikes had been broken into needle-shaped fragments under mechanical weathering.

automated Alphachron He extraction instrument (Applied Spectra, West Sacramento, CA, USA) was used to measure the ^{4}He concentrations.

Durango apatite was used as an analytical standard to check the analytical accuracy of the AHe ages. After degassing, the grains were dissolved in concentrated HNO_3 and HF acidic solutions and spiked with standards containing known quantities of U and Th. The ^{238}U, ^{235}U, ^{232}Th, and ^{147}Sm concentrations of each dissolved grain were measured using a Thermo Fisher Scientific Element 2 ICP-MS at the Institute of Geology of the Czech Academy of Sciences. The age of each grain was calculated using the standard radioactive decay equation standardized by Farley (2002), and the calculated ages were corrected by FT (Farley et al., 1996; Farley, 2002) to obtain the best ages (corrected ages).

2.5. AFT analysis:

Two samples were analyzed using AFT analysis at the Fission Track Laboratory of the Institute of Geology of the Czech Academy of Sciences, Prague.

The samples were mounted in epoxy resin, ground, and polished before etching. The samples were etched in 5.5 M HNO_3 for 20 s at 20 °C to reveal spontaneous tracks (Gleadow et al., 1986). They were then analyzed using the LA-FT method. The spontaneous track counts and the confined track length (TL) measurements were carried out in transmitted light at a magnification of 1000X with a fully motorized Zeiss Axioimager M1M microscope (Carl Zeiss NTS GmbH, Oberkochen, Germany) using TrackWorks software (v3.2.4; Melbourne University Fission Track Group, St, Carlton, Australia). ^{238}U measurements were done at the Geology Institute of the Czech Academy of Sciences, Prague (Czech Republic) using an Element 2 high-resolution sector field MS (Thermo Fisher Scientific) coupled with a 193-nm ArF Analyte Excite excimer LA system (Teledyne/Cetac; CETAC Technologies, Omaha, NE, USA) equipped with a HelEx II active 2-volume ablation cell (CETAC Technologies). The NIST 612 and NIST 610 glasses were used for calibration, and Durango (^{238}U:12 ppm) apatite was used as a secondary reference (Jochum et al., 2011). The LA-ICP-MS data were reduced using Iolite v.3.0 (Paton et al., 2011). Absolute age calibration was used to calculate single-grain AFT ages. Hasebe et al. (2004) was used to calculate the pooled ages, whereas the IsoplotR offline version was used to calculate the central ages and dispersion (Vermeesch, 2017; Vermeesch, 2018). Durango apatite is used to validate the counts and U content during the counting and U measurement sessions.

2.6. Thermal modelling

The thermal history models were calculated using QTQt (v.5.8.0) for each sample using inverse modeling based on the Bayesian trans-dimensional Markov chain Monte Carlo (MCMC) statistical method (Gallagher, 2012). The single grain age data, confined TL data with c-axis, and Dpar values of each sample were used as input values for the AFT data. Uncorrected ages, U, Th, Sm, and He amounts, and grain dimensions were used as input values for the AHe data. The inverse modelling ran 250,000 burn-in and 250,000 postburn-in iterations. The birth and death values of the MCMC run were similar, and the acceptance rates were between 0.2 and 0.5.

3. Analytical results

3.1 Petrography

The Eocene intrusions on Dismal Island included quartz diorite, tonalite, aplite, and micro gabbro. The quartz diorites were medium to coarse-grained with hypidiomorphic and slightly porphyritic texture and mainly composed of ~60–70 vol% plagioclase, ~5–7 vol% quartz, ~1–5 vol% K-feldspar, ~5–12 vol% pyroxene, ~0–8 vol % biotite, and ~2–5 vol% amphibole (Figure 4a). The plagioclase presented as euhedral to subhedral grains with polysynthetic twinning and showed considerable alteration to sericite, kaolinite, and rarely epidote. Although largely interstitial, K-feldspar was occasionally large enough to poikilitically include other minerals (especially pyroxene, biotite, and amphibole) and sometimes micrographic intergrowths with quartz (Figure 4b). Quartz was mainly an interstitial mineral and sometimes contained inclusions. Pyroxene was the most common ferromagnesian mineral and was invariably colorless. The clinopyroxene was observed as subhedral to anhedral grains. Some grains were occasionally altered to uralite and formed secondary amphiboles (Figure 4b; e.g., actinolite and green hornblende) along their rims. Brown biotite was found as both primary grains (Figure 4b) and an alteration product of the amphibole (e.g., hornblende). It had frequently partially chloritized and mantles clinopyroxene in places. Hornblende from the quartz diorites was mainly secondary to the clinopyroxenes. However, primary grains were also present to a lesser extent and partly replaced with chlorite along their rims. Accessory phases included sphene, apatite, zircon, Fe-Ti oxide, and epidote.

Tonalites had a mineralogy similar to the quartz diorites, except for the biotite. They were holocrystalline hypidiomorphic and medium to coarse-grained. They included ~65–70 vol% plagioclase, ~15–20 vol% quartz, ~1–5 vol% K-feldspar, ~1–5 vol% pyroxene, and ~5–10 vol% amphibole. Subhedral to anhedral plagioclases displayed mainly polysynthetic twinning and sometimes zoning. Alterations to the kaolinite, sericite, and epidote (Figure 4c) was common. The quartz crystals were both interstitial and had intergrown with K-feldspar and predominating plagioclase. The amount of clinopyroxene in the tonalites was less than that in the quartz diorites and was altered to hornblende and actinolite. Primary and secondary hornblende was abundant; the latter was an alteration product of the clinopyroxene and showed alteration to chlorite (Figure 4d). Other secondary and accessory phases included epidote, calcite, Fe-Ti oxide, apatite, sphene, and zircon.

The aplite dike samples from Dismal Island were fine to medium-grained and composed of subhedral to anhedral quartz, plagioclase, and K- feldspar (Figure 4e). They exhibited granular and micrographic textures. The feldspars were mainly altered to kaolinite and sericite (Figure 4e). The K-feldspars displayed a perthitic texture and Carlsbad twinning in places. Plagioclase was rarely replaced by myrmekite, and muscovite and Fe-Ti oxides were the accessory phases.

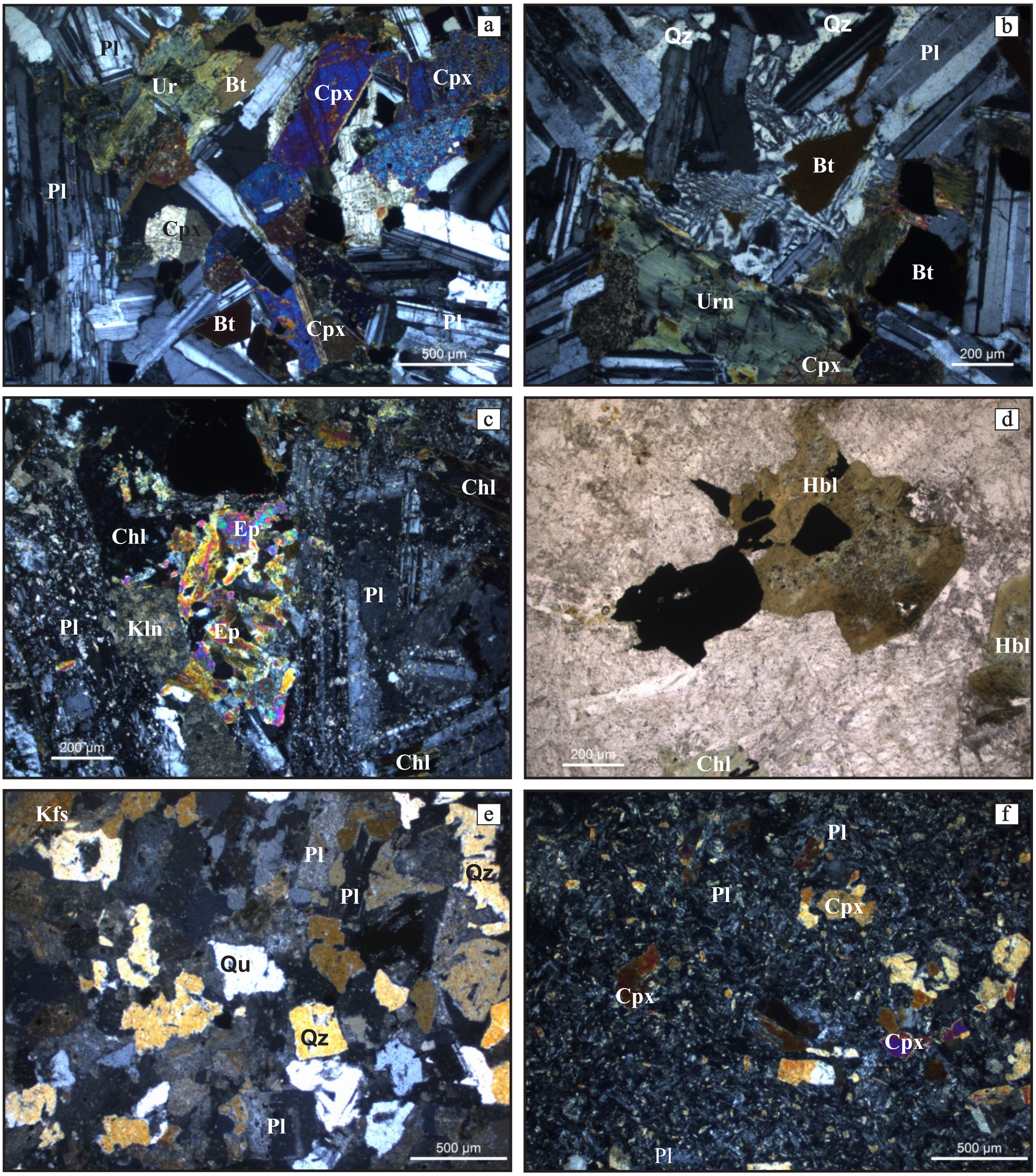

Figure 4. Representative petrographic features of different rocks from Dismal Island. (a) hypidiomorphic granular texture in quartz diorite defined by plagioclase (Pl), clinopyroxene (Cpx), and biotite (Bt); (b) micrographic intergrowth of K-feldspar (Kf), and quartz and uralitic amphibole (Urn) in quartz diorite; (c) epidote (Ep), chlorite (Chl), and kaolinite (Kln) in the altered tonalite; (d) brown hornblende and Fe-Ti oxide from tonalite with a granular texture; (e) aplite with a granular texture; (f) micro gabbro with a porphyritic texture, phenocrysts of the plagioclase and clinopyroxene set in a groundmass of finer plagioclase and clinopyroxene. Mineral abbreviations are from Whitney and Evans (2010).

The microgabbros samples from Dismal Island were fine-grained hypidiomorphic inequigranular with a porphyritic texture (Figure 4f). Mineral assemblages of the rocks consisted mainly of plagioclase (60–70 vol%) and clinopyroxene (25–35 vol%). The plagioclase displayed subhedral to anhedral crystals with albite and Carlsbad twinning. Some grains had partly altered to kaolinite and epidote, and clinopyroxenes mostly occurred as subhedral and anhedral grains. The aggregates of chlorite and epidote in the rocks were pseudomorphs of pyroxene and plagioclase, respectively.

3.2. Zircon U-Pb

Three samples were analyzed to determine the crystallization age of the magmatic intrusion. The results of the zircon U-Pb analyses are presented in the Supplementary file.

All of the samples included only shards of grains and the cathodoluminescence (CL) images showed oscillatory zoning indicating a magmatic origin (Figure 5) (Corfu et al., 2003). The samples had U ratios ranging from 138 to 2165 ppm for FK648, from 55 to 270 ppm for FK651, and from 131 to 3226 ppm for FK656, whereas the Th ratios ranged from 77 to 2746 ppm for FK648, from 26 to 265 ppm for FK651 and from 66 to 4474 ppm for FK656. The Th/U ratios range from 0.5 to 1.3 for FK648, from 0.4 to 0.9 for FK651, and from 0.5 to 1.3 for FK656 (Figure 6). These results also indicated a magmatic origin for all of the samples (Hoskin and Schaltegger, 2003; Yakymchuk et al., 2018).

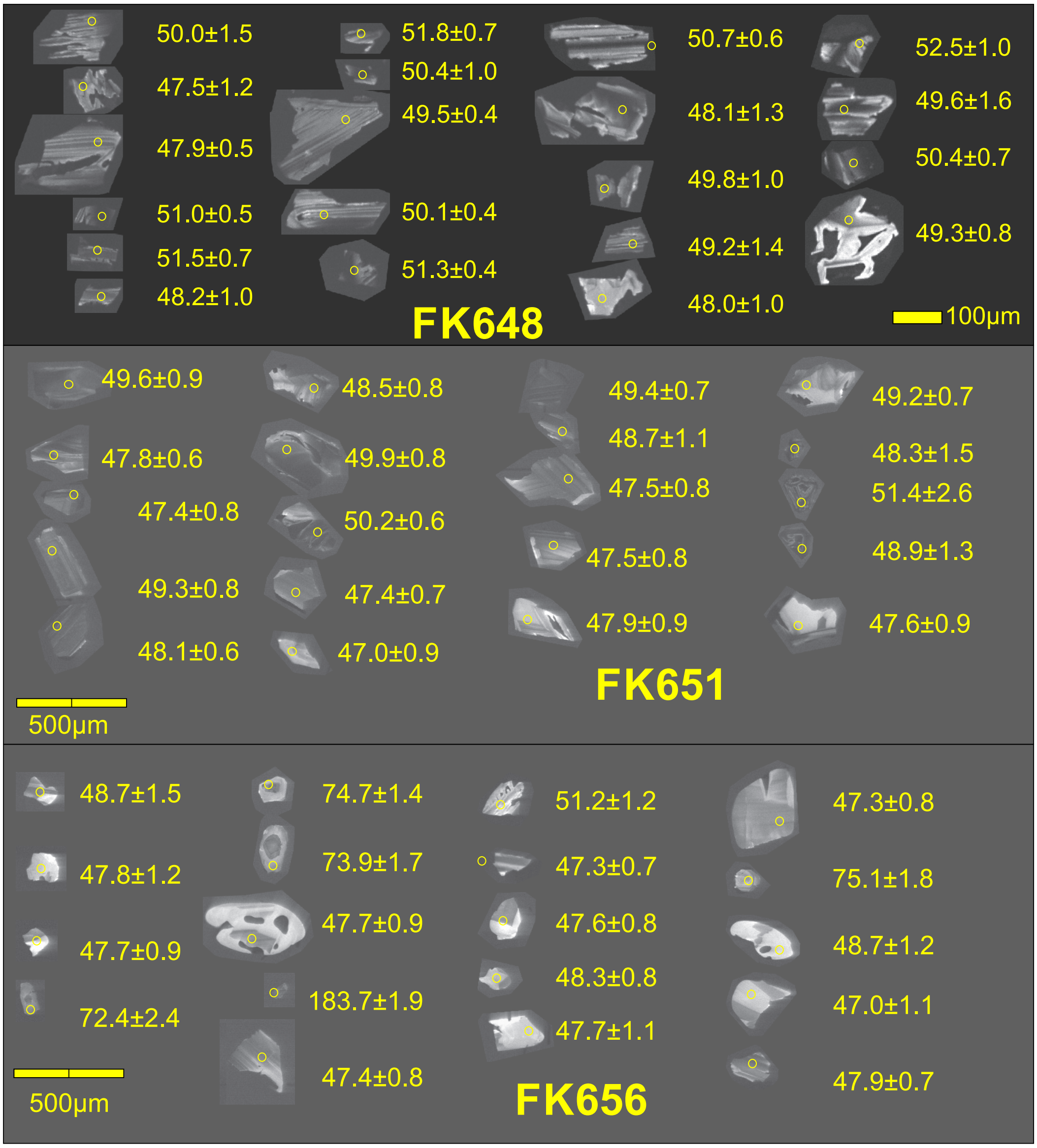

Figure 5. CL images of the analyzed samples.

Sample FK648 was collected from the topmost part of the island (Figure 2). The $^{206}Pb/^{238}U$ ages ranged from 47.2 to 52.5 Ma; however, the results showed that a significant number of the analyses indicated Pb loss, whereas the 4 concordant analyses yielded a crystallization age of 47.94 ± 0.5 Ma (mean squared weighted deviation [MSWD]: 0.87) (Figures 7a and 7b, Supplementary File). The analyzed zircon grains of sample FK651 were clustered into 2 groups. The $^{206}Pb/^{238}U$ ages of the group I ranged from 47 to 51.2 Ma, whereas the $^{206}Pb/^{238}U$ ages of the group II ranged from 72.4 to 75.1 Ma (Figures 7c and 7d, Supplementary File). Group I grain yielded a Concordia age of 47.76 ± 0.3 Ma (MSWD: 3.4, n = 10), and the group II zircons yielded a Concordia age of 74.5 ± 0.9 Ma (MSWD: 0.31, n = 3) (Figures 7c and 7d, Supplementary File). Sample FK656 was collected from the lowermost part of the island at sea level (Figure 2). The $^{206}Pb/^{238}U$ ages ranged from 47 to 51.4 Ma and yielded a Concordia age of 48.5 ± 0.2 Ma (MSWD: 1.6, n = 18) (Figures 7e and 7f, Supplementary File).

3.3. AFT

Two samples were analyzed using AFT thermochronology. Durango apatite was analyzed during the counting and LA-ICP-MS analyses to validate the counting and analyses. The Durango apatite yielded an AFT central age of 30.1 ± 1.8 Ma [31.0 ± 0.2 Ma, McDowell et al. (2005); 29.7 ± 1.9 Ma Hasebe et al. (2004)] (Table 2, Supplementary File).

The results are summarized in Table 2 and presented in Supplementary File. Both ages were significantly similar and yielded a late Eocene age. Sample FK651 yielded an AFT central age of 41.3 ± 2.9 Ma and a mean TL (MTL) of 12.19 μm (Table 2, Figure 8a, Supplementary File). The single-grain AFT ages passed the $\chi 2$ test, indicating a single population. Sample FK656 yielded an AFT central age of 41.8 ± 2.6 Ma and a MTL of 12.52 μm (Table 2, Figure 8b, Supplementary File). The single-grain AFT ages passed the $\chi 2$ test, indicating a single population.

3.4. AHe analysis

Sample FK656 (Q-diorite) was analyzed using AHe thermochronology. The AHe thermochronology referred to a temperature of ~60–70 °C, which may correspond to a depth of 2.5–3 km in the case of a normal geothermal gradient setting (30 °C/km). Five grains were analyzed for sample FK656 (Table 3). The eU values ranged between 11.85 and 65.54 (Table 3). The single-grain ages ranged from 18.31 to 21.49 (corrected ages) with a mean age of 20.01 ± 1.11 Ma (Table 3).

3.5. Thermal history modelling

The QTQt thermal history modeling results, shown in Figure 8, indicated that the sample entered the Partial Annealing Zone (PAZ) area shortly after crystallization. This may have resulted from either a shallow emplacement and a continued magmatic relaxation of the magmatic unit or the late Eocene uplift of the region.

The sample cooled to ~80 °C in a slow cooling phase starting in ~20 Ma, afterward, the sample cooled very rapidly in ~2 Ma, and was emplaced above a depth of ~2 km (Figure 8c). This rapid cooling may have resulted from the Middle-Miocene ridge-trench collision between the Tula and Adelaide fracture zones and/or the opening of the slab window beneath the region. The TL distribution of the sample had a bimodal length distribution, indicating an episodic slow cooling phase (Figure 8d) (Gleadow et al., 1983).

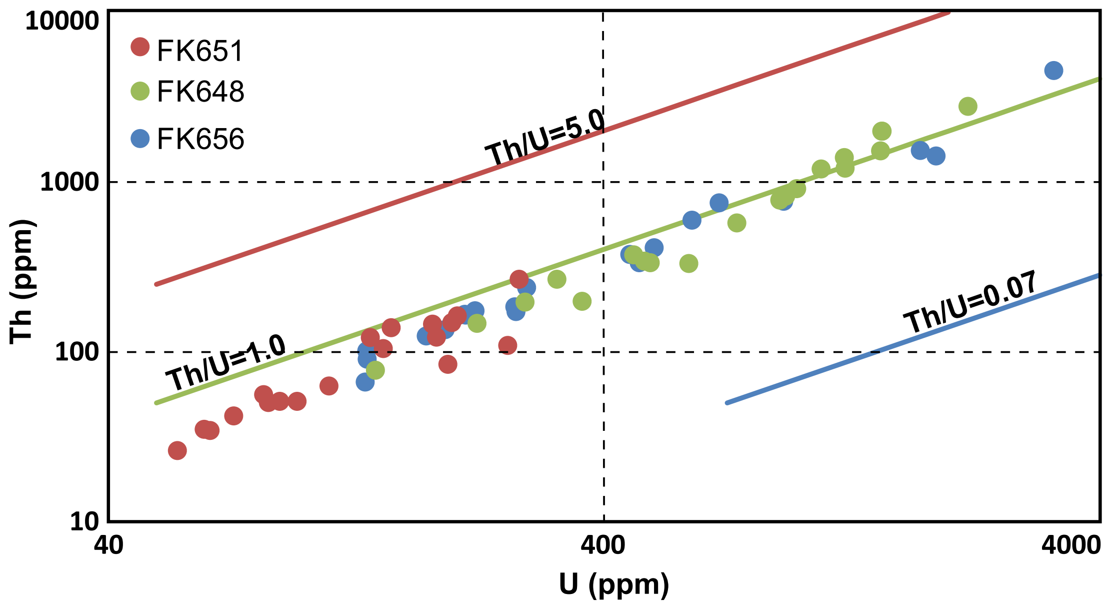

Figure 6. Th vs. U abundances of the analyzed zircon grains of all of the samples.

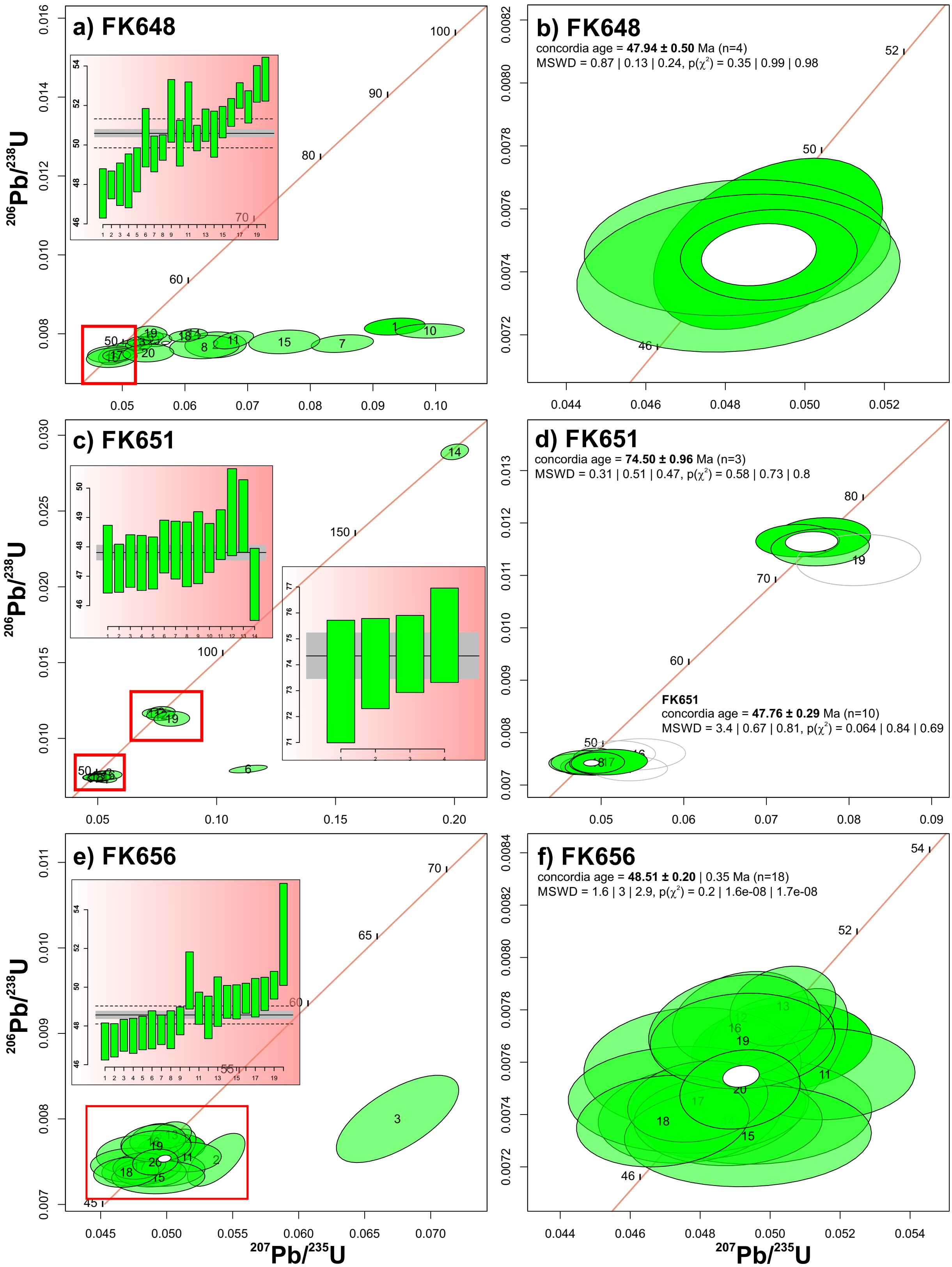

Figure 7. U-Pb Concordia diagrams of the analyzed samples.

Table 2. Summary of the AFT analytical data for Dismal Island.

Sample number	No. of grains	Ns	ρs (10^5 cm^{-2})	238U (µg/g)	Pooled age (Ma ± 1σ)	Central age (Ma ± 1σ)	P (χ2)	NL	MTL (µm ± SE)	SD (µm)	Dpar (µm)
FK651	62	815	1.62	8.43	39.1 ± 2.9	41.3 ± 2.9	0.28	23	12.19	2.38	2.49
FK656	63	1052	1.47	6.96	39.4 ± 2.6	41.8 ± 2.6	0.85	56	12.52	2.95	2.57
Dur	31	1231				30.2 ± 1.8	0.83				

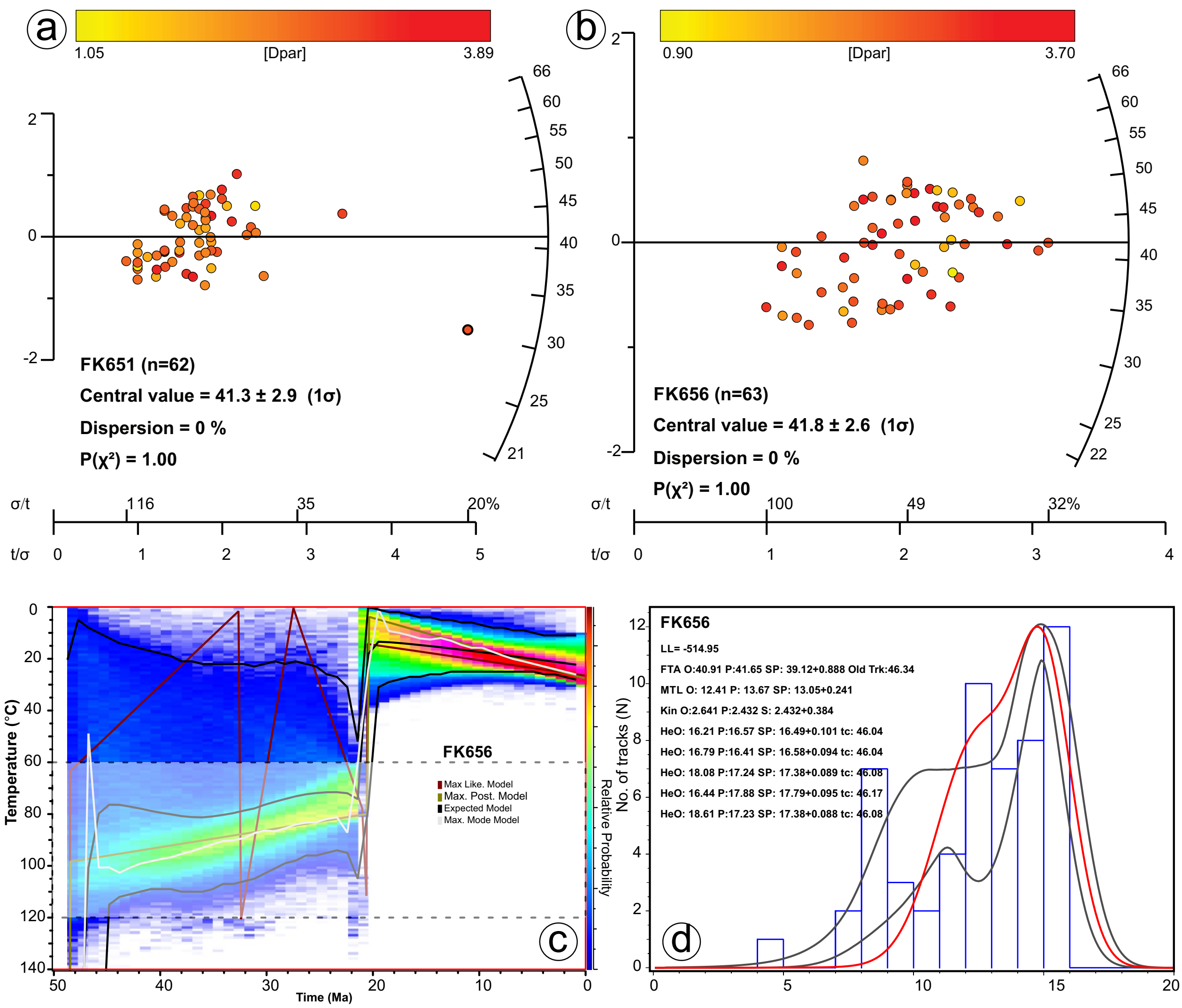

Figure 8. (a, b) AFT radial plots of the samples from Dismal Island. The single-grain AFT age spot colors correspond to their Dpar values. N: number of analyzed apatite grains; P(χ2): chi-squared probability test; (c, d) thermal history modeling and TL distribution histogram of the sample FK656 (see the text for details).

Table 3. Summary of the apatite (U-Th)/He data for sample FK656.

Sample number	4He (nmol)	Mass (µg)	FT	U (µg/g)	Th (µg/g)	Sm (µg/g)	Th/U	Eu (µg/g)	Uncorr. Age (Ma)	Corr. Age (Ma)	± 1σ (Ma)	L (µm)	W (µm)	H (µm)
FK656-1	1.51E-04	2.68	0.84	39.06	111.62	223.57	2.84	65.54	16.22	**19.38**	**0.21**	142.0	113.9	277.0
FK656-2	1.15E-04	8.45	0.84	9.11	27.24	52.11	3.01	15.44	16.79	**20.04**	**0.22**	136.1	123.7	253.9
FK656-11	2.43E-04	16.58	0.87	8.90	27.00	61.73	3.06	15.18	18.08	**20.83**	**0.20**	272.2	167.0	156.1
FK656-12	3.38E-04	32.24	0.90	7.02	20.80	45.69	2.99	11.85	16.44	**18.31**	**0.17**	313.9	219.9	196.8
FK-656-3	2.52E-04	14.27	0.87	10.28	31.92	67.34	3.13	17.71	18.61	**21.49**	**0.20**	237.8	166.3	153.9
										20.01	**1.11**			

FT: alpha ejection correction after Farley et al. (1996); Eu: effective uranium concentration (U ppm + 0.235 Th ppm); L: grain length, W: grain width, and H: grain height.

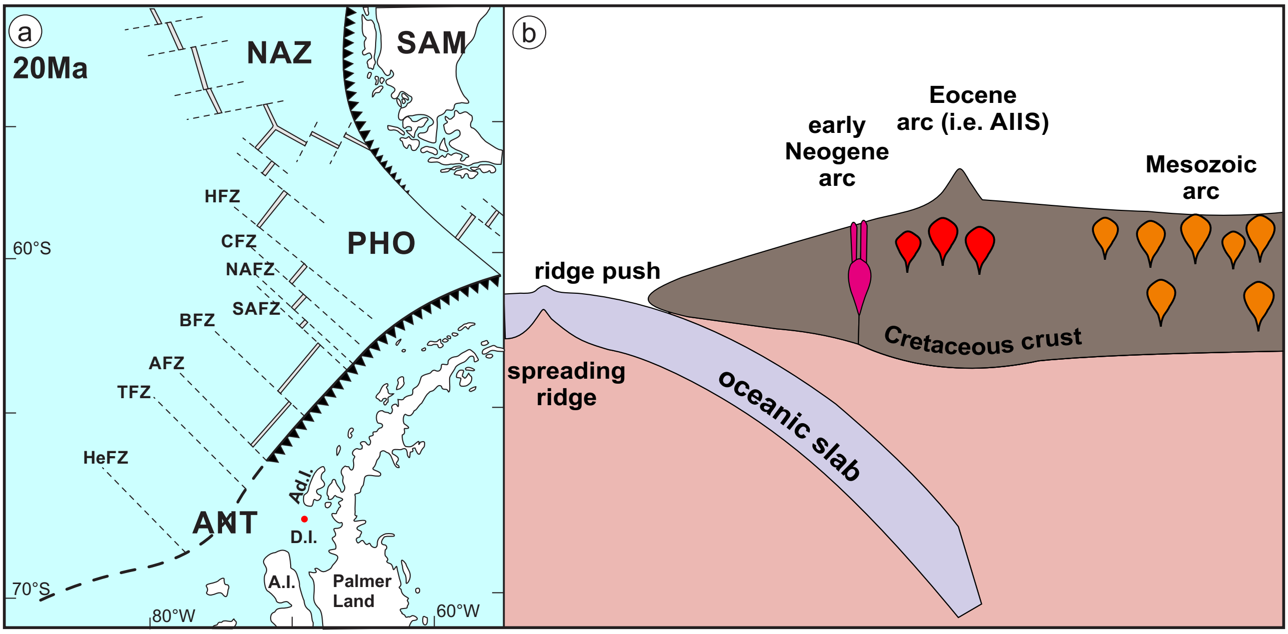

Figure 9. (a) 20 Ma reconstruction of the southeast Pacific; (b) geodynamic model along the Adelaide Island showing the age and migration of arc magmatism. Ad.I.: Adelaide Island; A.I.: Alexander Island; ANT: Antarctic Plate; AFZ: Adelaide Fracture Zone; BFZ: Biscoe Fracture Zone; CFZ: C Fracture Zone; HeFZ: Heezen Fracture Zone; HFZ: Hero Fracture Zone; NAFZ: North Anvers Fracture Zone; NAZ: Nazca Plate; SAM: South American Plate; PHO: Phoenix Plate; SCO, Scotia Plate; SAFZ: South Anvers Fracture Zone; SHET: South Shetlands microplate; TFZ: Tula Fracture Zone (Hole and Larter, 1993; Johnson, 1997; Larter et al., 1997; Guenthner et al., 2010; Jordan et al., 2014).

4. Results and discussion

The AP has witnessed continuous subduction, accretion, and collision events since the Paleozoic (Vaughan and Storey, 2000; Burton Johnson and Riley, 2015; Bastias et al., 2020; Jordan et al., 2020; Storey and Granot, 2021). The plutonic rocks were grouped under the AP batholith, one of the major batholiths of the circum-Pacific rim, which covers the whole region with ages ranging from Paleozoic to Cenozoic (Leat et al., 1995). Geophysical studies have suggested a ~1500-km-long positive magnetic Pacific Margin Anomaly associated with the Cretaceous arc batholith (Storey and Garrett, 1985; Leat et al., 1995). The Eocene magmatism is outcropped on Adelaide and Alexander islands, similar to those on Dismal Island (Griffiths and Oglethorpe, 1998; Riley et al., 2012). The magmatic body intruded into the Cretaceous crust, which also formed in the same subduction environment and belongs to the AP batholith. To the north of Adelaide Island, the age of the magmatism on Sillar Island was dated to the earliest Miocene (22.9 ± 0.2), reflecting that the arc magmatism has continued since this period (Jordan et al., 2014). The first uplift of the region occurred during the Late Eocene in an arc setting (Figure 9).

The Cenozoic tectonic environment is marked by the northward migration of subduction of the Antarctic-Phoenix spreading center and the ridge-trench collision along the northern margin of the peninsula. The subducted ridge let open a slab window beneath the overriding plate, causing crustal heating and uplift of the region due to asthenospheric upwelling (Figure 9). The current research data supports that continuing subduction and ridge-trench collision caused a fast uplift of the region during Burdigalian.

The analytical results obtained in this study suggest the following:

- The magmatic suite on Dismal Island consists of tonalite, Q-diorite, gabbro, aplite, and micro gabbro.
- The formation age of magmatic suite outcrops on Dismal Island is restricted to Ypresian (48–47 Ma), where the magmatism was emplaced in an Upper Cretaceous lower crust.
- Similar magmatic rocks are outcropped on Adelaide Island, which were named the Adelaide Island Intrusive Suite.
- The AFT ages indicated a Bartonian-Lutetian (41–39) uplift in the region. Similar AFT ages were also found on Adelaide and Alexander islands and on the archipelagos close to Adelaide Island, suggesting that the continuing subduction uplifted the whole region during this period.
- The cooling profile showed a slow cooling phase between 40 and ~20 Ma, which reflects a steady-state setting in the region during Bartonian and Burdigalian.
- The Ahe age and the cooling profile indicated a rapid uplift in ~20 Ma. This fast uplift resulted from the ridge-trench collision and opening of the slab-window beneath the overriding plate along the continental shelf between the Tula and Adelaide fracture zones.

Acknowledgments

This study was carried out under the auspices of the Presidency of The Republic of Türkiye, supported by the Ministry of Industry and Technology, and coordinated by The Scientific and Technological Research Council of Türkiye (TÜBİTAK) MAM Polar Research Institute under project number: TÜBİTAK-121Y357. The authors thank the TAE-VI members for their support in the field.

Supplementary material

https://aperta.ulakbim.gov.tr/record/263287

References

Bastias J, Spikings R, Ulianov A, Riley T, Burton Johnson A et al. (2020). The Gondwanan margin in West Antarctica: insights from Late Triassic magmatism of the Antarctic Peninsula. Gondwana Research 81: 1-20.

Breitsprecher K, Thorkelson DJ (2009). Neogene kinematic history of Nazca–Antarctic–Phoenix slab windows beneath Patagonia and the Antarctic Peninsula. Tectonophysics 464: 10-20.

Burton Johnson A, Riley TR (2015). Autochthonous v. accreted terrane development of continental margins: a revised in situ tectonic history of the Antarctic Peninsula. Journal of the Geological Society 172: 822-835.

Butterworth PJ, Crame JA, Howlett PJ, Macdonald DIM (1988). Lithostratigraphy of Upper Jurassic-Lower Cretaceous strata of eastern Alexander Island, Antarctica. Cretaceous Research 9: 249-264.

Clinger AE, Fox M, Balco G, Cuffey K, Shuster DL (2020). Detrital thermochronometry reveals that the topography along the Antarctic Peninsula is not a Pleistocene landscape. Journal of Geophysical Research: Earth Surface 125: e2019JF005447.

Corfu F, Hanchar JM, Hoskin PWO, Kinny P (2003). Atlas of zircon textures. In: Finch RJ, Hanchar JM (editors). Zircon. Reviews in Mineralogy and Geochemistry, pp. 469-500.

Dalziel IWD (1982). West Antarctica – problem child of Gondwanaland. Tectonics 1: 3-19.

Doubleday PA, Macdonald DIM, Nell PAR (1993). Sedimentology and structure of the trench-slope to forearc basin transition in the Mesozoic of Alexander Island, Antarctica. Geological Magazine 130: 737-754.

Eagles G (2004). Tectonic evolution of the Antarctic-Phoenix plate system since 15 Ma. Earth and Planetary Science Letters 217: 97-109.

Farley KA, Wolf RA, Silver LT (1996). The effects of long alpha-stopping distances on (U-Th)/He ages. Geochimica et Cosmochimica Acta 60: 4223-4229.

Farley KA (2002). (U-Th)/He dating: techniques, calibrations, and applications. In: Porcelli DP, Ballentine CJ, Wieler R (editors). Noble Gases in Geochemistry and Cosmochemistry. Reviews in Mineralogy and Geochemistry pp. 819-844.

Gallagher K (2012). Transdimensional inverse thermal history modeling for quantitative thermochronology. Journal of Geophysical Research: Solid Earth 117: B2.

Gleadow AJW, Duddy IR, Lovering JF (1983). Fission track analysis: A new tool for the evaluation of thermal histories and hydrocarbon potential. The APPEA Journal 23: 93-102.

Gleadow AJW, Duddy IR, Green PF, Lovering JF (1986). Confined fission track lengths in apatite: a diagnostic tool for thermal history analysis. Contributions to Mineralogy and Petrology 94: 405-415.

Griffiths CJ, Oglethorpe RDJ (1998). The stratigraphy and geochronology of Adelaide Island. Antarctic Science 10: 462-475.

Guenthner WR, Barbeau Jr. DL, Reiners PW, Thomson SN (2010). Slab window migration and terrane accretion preserved by low-temperature thermochronology of a magmatic arc, northern Antarctic Peninsula. Geochemistry, Geophysics, Geosystems 11.

Hasebe N, Barbarand J, Jarvis K, Carter A, Hurford AJ (2004). Apatite fission-track chronometry using laser ablation ICP-MS. Chemical Geology 207: 135-145.

Hole MJ, Larter RD (1993). Trench-proximal volcanism following ridge crest-trench collision along the Antarctic Peninsula. Tectonics 12: 897-910.

Hole MJ, Saunders AD, Rogers G, Sykes MA (1994). The relationship between alkaline magmatism, lithospheric extension and slab window formation along continental destructive plate margins. Geological Society, London, Special Publications 81: 265-285.

Hoskin PWO, Schaltegger U (2003). The composition of zircon and igneous and metamorphic petrogenesis. In: Finch RJ, Hanchar, JM (editors). Zircon. Reviews in Mineralogy and Geochemistry pp. 27-62.

Johnson AC (1997). Cenozoic tectonic evolution of the Marguerite Bay area, Antarctic Peninsula, interpreted from geophysical data. Antarctic Science 9: 268-280.

Jordan TA, Neale RF, Leat PT, Vaughan APM, Flowerdew MJ et al. (2014). Structure and evolution of Cenozoic arc magmatism on the Antarctic Peninsula: a high resolution aeromagnetic perspective. Geophysical Journal International 198: 1758-1774.

Jordan TA, Riley TR, Siddoway CS (2020). The geological history and evolution of West Antarctica. Nature Reviews Earth and Environment 1: 117-133.

Larter RD, Rebesco M, Vanneste LE, GambôA LAP, Barker PF (1997). Cenozoic tectonic, sedimentary and glacial history of the Continental Shelf west of Graham Land, Antarctic Peninsula. In: Barker PF, Cooper AK (editors). Geology and Seismic Stratigraphy of the Antarctic Margin, 2, pp. 1-27.

Lawver LA, Gahagan LM, Coffin MF (1992). The development of paleoseaways around Antarctica. In: Kennett JP, Warkne DA (editors). The Antarctic Paleoenvironment: A Perspective on Global Change: Part One, pp. 7-30.

Leat PT, Scarrow JH, Millar IL (1995). On the Antarctic Peninsula batholith. Geological Magazine 132: 399-412.

Macdonald DIM, Leat PT, Doubleday PA, Kelly SRA (1999). On the origin of fore-arc basins: new evidence of formation by rifting from the Jurassic of Alexander Island, Antarctica. Terra Nova 11: 186-193.

McDowell FW, McIntosh WC, Farley KA (2005). A precise Ar-40-Ar-39 reference age for the Durango apatite (U-Th)/He and fission-track dating standard. Chemical Geology 214: 249-263.

Millar IL, Pankhurst RJ, Fanning CM (2002). Basement chronology of the Antarctic Peninsula: recurrent magmatism and anatexis in the Palaeozoic Gondwana Margin. Journal of the Geological Society 159: 145-157.

Riley TR, Flowerdew MJ, Whitehouse MJ (2012). Chrono- and lithostratigraphy of a Mesozoic–Tertiary fore- to intra-arc basin: Adelaide Island, Antarctic Peninsula. Geological Magazine 149: 768-782.

Riley TR, Leat PT (2021). Chapter 2.2b Palmer Land and Graham Land volcanic groups (Antarctic Peninsula): petrology. Geological Society, London, Memoirs 55: 139-156.

Storey BC, Garrett SW (1985). Crustal growth of the Antarctic Peninsula by accretion, magmatism and extension. Geological Magazine 122: 5-14.

Storey BC, Nell PAR (1988). Role of strike-slip faulting in the tectonic evolution of the Antarctic Peninsula. Journal of the Geological Society 145: 333-337.

Storey BC, Brown RW, Carter A, Doubleday PA, Hurford AJ et al. (1996). Fission-track evidence for the thermotectonic evolution of a Mesozoic-Cenozoic fore-arc, Antarctica. Journal of the Geological Society 153: 65-82.

Storey BC, Granot R (2021). Chapter 1.1 Tectonic history of Antarctica over the past 200 million years. Geological Society, London, Memoirs 55: 9-17.

Twinn G, Riley T, Fox M, Carter A (2022). Thermal history of the southern Antarctic Peninsula during Cenozoic oblique subduction. Journal of the Geological Society 179.

Vaughan APM, Storey BC (2000). The eastern Palmer Land shear zone: a new terrane accretion model for the Mesozoic development of the Antarctic Peninsula. Journal of the Geological Society London 157: 1243-1256.

Vaughan APM, Eagles G, Flowerdew MJ (2012). Evidence for a two-phase Palmer Land event from crosscutting structural relationships and emplacement timing of the Lassiter Coast Intrusive Suite, Antarctic Peninsula: Implications for mid-Cretaceous Southern Ocean plate configuration. Tectonics 31.

Vermeesch P (2017). Statistics for LA-ICP-MS based fission track dating. Chemical Geology 456: 19-27.

Vermeesch P (2018). IsoplotR: A free and open toolbox for geochronology. Geoscience Frontiers 9: 1479-1493.

Whitney DL, Evans BW (2010). Abbreviations for names of rock-forming minerals. American Mineral 95: 185-187.

Willan RCR (2003). Provenance of Triassic-Cretaceous sandstones in the Antarctic Peninsula: implications for terrane models during Gondwana breakup. Journal of Sedimentary Research 73: 1062-1077.

Wyeth RB (1977). The physiography and significance of the transition zone between Graham Land and Palmer Land. British Antarctic Survey Bulletin 46: 39-58.

Yakymchuk C, Kirkland CL, Clark C (2018). Th/U ratios in metamorphic zircon. Journal of Metamorphic Geology 36: 715-737.